energies

MDPI

Article

Fractal and Multifractal Analysis of Pore Size Distribution in Low Permeability Reservoirs Based on Mercury Intrusion Porosimetry

Penghui Su [1,*], Zhaohui Xia [1], Ping Wang [1], Wei Ding [1], Yunpeng Hu [1], Wenqi Zhang [1] and Yujie Peng [2]

1 PetroChina Research Institute of Petroleum Exploration and Development, Beijing 100083, China; xiazhui@petrochina.com.cn (Z.X.); wp2011@petrochina.com.cn (P.W.); dingwei-hw@petrochina.com.cn (W.D.); huyunpeng1129@petrochina.com.cn (Y.H.); zhang_wenqi@petrochina.com.cn (W.Z.)

2 Guizhou Polytechnic of Construction, Guizhou 551400, China; pyjcumt@126.com

* Correspondence: suphui317@petrochina.com.cn; Tel.: +86-150-105-669-36

Received: 3 March 2019; Accepted: 29 March 2019; Published: 8 April 2019

Abstract: To quantitatively evaluate the complexities and heterogeneities of pore structures in sandstone reservoirs, we apply single fractal theory and multifractal theory to explore the fractal characteristics of pore size distributions based on mercury intrusion porosimetry. The fractal parameters were calculated and the relationships between the petrophysical parameters (permeability and entry pressure) and the fractal parameters were investigated. The results show that the single fractal curves exhibit two-stage characteristics and the corresponding fractal dimensions D_1 and D_2 can characterize the complexity of pore structure in different sizes. Favorable linear relationships between $\log(\varepsilon)$ and $\log(\mu,(\varepsilon))$ indicate that the samples satisfy multifractal characteristics and ε is the sub-intervals with size $\varepsilon = J \times 2^{-k}$. The multifractal singularity curves used in this study exhibit a right shape, indicating that the heterogeneity of the reservoir is mainly affected by pore size distributions in sparse regions. Multifractal parameters, $D(0)$, $D(1)$, and Δf, are positively correlated with permeability and entry pressure, while $D(0)$, $D(1)$, and Δf are negatively correlated with permeability and entry pressure. The ratio of larger pores volumes to total pore volumes acts as a control on the fractal dimension over a specific pore size range, while the range of the pore size distribution has a definite impact on the multifractal parameters. Results indicate that fractal analysis and multifractal analysis are feasible methods for characterizing the heterogeneity of pore structures in a reservoir. However, the single fractal models ignore the influence of microfractures, which could result in abnormal values for calculated fractal dimension. Compared to single fractal analysis, multifractal theory can better quantitatively characterize the heterogeneity of pore structure and establish favorable relationships with reservoir physical property parameters.

Keywords: multifractal theory; fractal theory; pore structure; mercury intrusion porosimetry; pore size distribution

1. Introduction

A reservoir consists of a complex porous medium composed of pores with different origins, irregular shapes, and self-similarities. The pore structure in a reservoir is mainly affected by three factors: sedimentation, diagenesis, and tectogenesis. Each of these factors result in the formation of pores with attributes which fall into different ranges. Thus, different types of pores are formed and exist in the reservoir in a certain distribution. This complex pore size distribution is dynamically nonlinear and is the result of numerous processes occurring at various scales [1].

Fractal theory, a promising tool for investigating complex structures, has been widely used to quantitatively characterize the complexities and heterogeneities of pore size distributions [2]. Fractal theory is considered to be an effective means of quantitatively depicting irregular shapes, and can accurately express the complexity and heterogeneity of geological bodies. Extensive research has proven that reservoirs exhibit fractal characteristics. Pfeifer found that the pore surface area of a reservoir exhibits fractal characteristics by the using molecular adsorption [3]. Katz investigated different types of sandstone using scanning electron microscopy; the results indicated that the pore spaces of sandstone possess fractal characteristics [4]. Friesen obtained the fractal dimensions of coal particles based on capillary injection data [5].

Mercury intrusion porosimetry is commonly used to determine the pore structure distributions of rocks [6]. Fractal studies of capillary pressure data mainly focus on obtaining fractal dimensions to establish the relationship between fractal dimension and reservoir physical properties [7,8]. There are several widely used fractal models to obtain the fractal dimension of mercury injection data based on single fractal theory [5,9–11]. Single fractal theory describes the integrity characteristics of pore structures [7]; it is suitable for application to a homogeneous reservoir, but cannot define the local pore structure or reflect other comprehensive and detailed information [12]. The segmented fractal phenomenon occurs when the fractal theory is applied to mercury injection data [13–15]. This fact demonstrates that describing the complexity of the whole pore system is difficult with a single fractal dimension.

Multifractal analysis was conducted to describe the complexity of pore size distribution because single fractal theory has limitations in describing the local characteristics of pore size distribution. Multifractal theory partitions objects at different scales to obtain distribution characteristics [16,17]. As a result, it likely characterizes the complex and heterogeneous behavior of a reservoir more effectively than the single fractal theory [7]. Multifractal theory has been widely applied to study effect of pore size changes on reservoir physical properties [18]. Multifractal analysis of soil pore structure has been widely studied to characterize soil structure stability and soil surface evolution stages [19]. Multifractal theory has also been confirmed as a useful tool for characterizing the internal complexity and amplifying the differences in pore size distributions between different coals [1]. Research on the quantitative characterization of the irregular microscopic pore structures of different rock types has been performed on the basis of 2-D images [20–23]. From the above literature review, we can conclude that multifractal analysis of pore size distribution measured by mercury intrusion porosimetry has not been extensively applied to sandstone reservoirs. Comparative studies of single fractal theory and multifractal theory based on mercury intrusion porosimetry have not been performed.

In the present study, single fractal theory and multifractal theory are applied to investigate variability and heterogeneity in pore structures based on mercury intrusion curves. Single fractal and multifractal parameters were analyzed for correlation with reservoir physical parameters. We compared single fractal theory and multifractal theory to test which method is more suitable for characterizing reservoir physical parameters. Multifractal analysis of pore structures can expand our understanding of the pore structures of reservoirs.

2. Materials and Methods

2.1. Single Fractal Theory

Several fractal models were established to obtain the fractal dimensions of mercury injection data. Su's fractal model, which considers both the fractal characteristics of pore space and pore length and was proposed based on the capillary bundle model, was applied in this paper [11]:

$$\log(S_{Hg}) \propto \left(D_f + D_T - 3\right) \log(P_c) \tag{1}$$

where S_{Hg} is the mercury saturation, D_f is the fractal dimension for pore space, with $2 < D_f < 3$ in three dimensions [24], D_T is the fractal dimension for tortuosity, with $1 < D_T < 3$ in three dimensions [25], and P_c is the capillary pressure. The sum of the fractal dimension of pore space and the fractal dimension of tortuosity can be obtained from the double logarithmic curve of mercury saturation and capillary pressure. Theoretically, the sum of the fractal dimensions of pore space and tortuosity should be between 3 and 6; the larger the sum of fractal dimension, the more complicated the pore structure [11].

2.2. Multifractal Theory

Multifractal theory describes the local conditions of a fractal structure through the singularity strength [26], and the overall characteristics are investigated from a local perspective. The prerequisite for applying the multifractal analysis method is that the measurement interval must be divided equally [27].

The mercury injection curves obtained in this study have fewer measurement points than is required for the multifractal method. To obtain enough data for multifractal analysis of mercury intrusion curves, we used cubic spline interpolation to interpolate mercury intrusion curves, allowing us to obtain more data points.

In this study, the whole measured pore size was defined as I, I = [0.015, 35.6 μm]. The difference of capillary pressure data in the aforementioned pore size range is measured over steps of 0.005 μm. Thus, sub-intervals can be obtained. I_i represents the i-th sub-interval, and ν_i represents the percentage of pore volume in the sub-interval I_i. A new measure can be obtained (J = [log0.015, log35.6 μm]) by plotting the aforementioned pore size range I on a logarithmic scale. J was divided into 2^k equal sub-intervals with size $\varepsilon = J \times 2^{-k}$. The whole interval is divided into reduced sub-intervals with increasing k; thus, the effects of pore space changes within a small interval can be investigated. J_i represents the i sub-interval in the interval J. $P_i(\varepsilon)$ represents the percentage of pore volume in the sub-interval J_i; it is equal to the sum of ν_i that falls within the sub-interval J_i.

The partition function $\chi(q,\varepsilon)$ can be defined using $P_i(\varepsilon)$:

$$\chi(q,\varepsilon) = \sum_{i=1}^{N(\varepsilon)} P_i(\varepsilon)^q \tag{2}$$

where q is a real parameter that describes the moment order of the measure. For $q < 1$, $\chi(q,\varepsilon)$ emphasizes the regions determined by a small $P_i(\varepsilon)$ or minimally concentrated region of a measure. For $q > 1$, $\chi(q,\varepsilon)$ emphasizes the regions determined by a large $P_i(\varepsilon)$ or wide concentrated region of a measure. The q used in this study is between −20 and 20. $\chi(q,\varepsilon)$ and ε follow a power law relationship as follows:

$$\chi(q,\varepsilon) \propto \varepsilon^{\tau(q)} \tag{3}$$

where $\tau(q)$ is the mass exponent, which can also be expressed by the following formula:

$$\tau(q) = \lim_{\varepsilon \to 0} \frac{\lg(\sum_{i=1}^{N(\varepsilon)} P_i(\varepsilon)^q)}{\lg(\varepsilon)} \tag{4}$$

The mass exponent can also be expressed as follows, according to previous research results [19]:

$$\tau(q) = (q-1)D(q) \tag{5}$$

where $D(q)$ is the generalized dimension. Correspondingly, $D(q)$ can be expressed as follows:

$$D(q) = \lim_{\varepsilon \to 0} \frac{1}{q-1} \frac{\lg(\sum_{i=1}^{N(\varepsilon)} P_i(\varepsilon)^q)}{\lg(\varepsilon)} (q \neq 1), \tag{6}$$

For $q = 1$, $D(q)$ is defined as follows [26]:

$$D(1) = \lim_{\varepsilon \to 0} \left\{ \frac{\sum_{i=1}^{N(\varepsilon)} \mu_i(\varepsilon) \log(\mu_i(\varepsilon))}{\lg(\varepsilon)} \right\} \tag{7}$$

If ε is sufficiently small, then $P_i(\varepsilon)$ is nearly evenly distributed within each subinterval, where $P_i(\varepsilon)$ and ε show the following relationship:

$$P_i(\varepsilon) \propto \varepsilon^{\alpha} \tag{8}$$

where α is the singularity exponent. Different subintervals may have the same α. $N_\alpha(\alpha)$ represents the subinterval numbers of the singularity exponent between α and $\alpha + d\alpha$; it satisfies the following fractal power law relationship:

$$N_\alpha(\varepsilon) \propto \varepsilon^{-f(\alpha)} \tag{9}$$

where $f(\alpha)$ is a multifractal spectrum with singularity exponent α. Different α values and corresponding $f(\alpha)$ constitute the multifractal spectrum that describes multifractal properties.

The singularity exponent can also be expressed as follows:

$$\alpha(q) = \lim_{\varepsilon \to 0} \frac{\sum_{i=1}^{N(\varepsilon)} \mu_i(q,\varepsilon) \lg(P_i(\varepsilon))}{\lg(\varepsilon)} \tag{10}$$

The multifractal spectrum of pore distribution $f(\alpha)$ relative to α is defined as follows:

$$f[\alpha(q)] = \lim_{\varepsilon \to 0} \frac{\sum_{i=1}^{N(\varepsilon)} \mu_i(q,\varepsilon) \lg \mu_i(q,\varepsilon)}{\lg(\varepsilon)} \tag{11}$$

The first step of the multifractal analysis of capillary pressure data is to interpolate mercury intrusion curves to obtain sufficient points. The equidistant division of a logarithmic pore size range is the basis for obtaining the probability density $P_i(\varepsilon)$ and the partition function $\chi(q,\varepsilon)$. $\tau(q)$, $D(q)$, $\alpha(q)$, and $f(q)$ can be obtained from Equations (2), (4), (6), (10) and (11), respectively. $\tau(q)$ and $D(q)$ describe the multifractal characteristics, whereas $\alpha(q)$, and $f(q)$ characterize the local characteristics of the multifractal structure.

3. Samples and Experiments

A total of 13 samples were obtained from a well located in Western Sichuan, China. The physical properties of the samples are relatively variable (Figure 1), which is convenient for comparison using multifractal analysis. All samples were tested for porosity, and permeability and subjected mercury injection experiments in accordance with Chinese Petroleum Industry Standards SY/T 6385-1999 and SY/T 5346-2005.

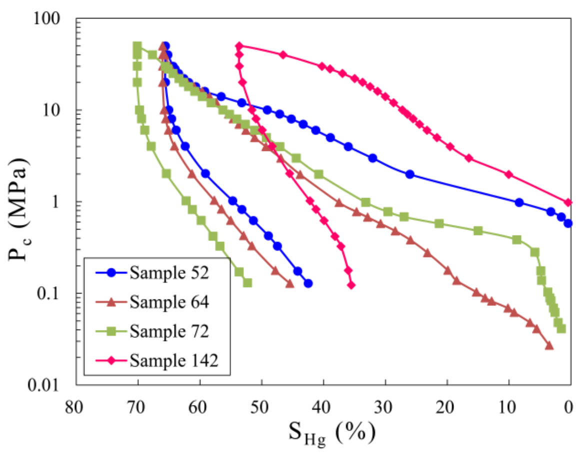

Figure 1. Four typical mercury intrusion curves.

Porosity and permeability were obtained using routine rock property measurement techniques. The average permeability is 6.11 mD; the range extends from 0.14 mD to 42.29 mD. The average porosity is 11.59%; it ranges from 6.31% to 16.65%. The experimental results are summarized in Table 1. The entry pressure (the point on the curve at which the mercury first enters the pores of the samples) varies from 0.037 MPa to 1.450 MPa, with an average of 0.726 MPa. r_{50} varies from 0.018 µm to 0.247 µm, with an average of 0.089 µm. An analysis of physical properties shows that the reservoir exhibits strong heterogeneity and complexity in its microscopic pore structure.

Table 1. Parameters of the pore throat structure obtained from the 13 samples.

Samples	Permeability	Porosity	Entry Pressure	Sorting Coefficient	r_{50}
	mD	%	MPa		um
9	0.3250	13.3547	1.0760	1.6867	0.0415
13	0.1420	7.2449	1.4070	1.5212	0.0186
22	5.0690	12.2603	0.2350	2.5778	0.1444
37	1.1000	14.0306	1.0030	1.8189	0.0956
46	0.5730	12.3959	1.2150	1.4568	0.2471
52	1.5060	8.1072	0.8450	1.9145	0.0706
64	42.2990	16.6477	0.0370	3.3595	0.1688
72	16.5960	11.2793	0.1900	2.6728	0.1367
81	0.8070	13.3353	0.6400	2.1086	0.0762
93	4.8510	14.9307	0.1970	2.6960	0.0285
105	5.3600	11.0967	0.1880	2.5586	0.0848
142	0.5420	6.3134	1.4500	1.4509	0.0165
146	0.2420	9.6940	0.9620	1.7438	0.0320

Note: r_{50} corresponds to pore throat diameter at 50% mercury saturation; Sorting coefficient is the dispersion degree of reservoir pores.

The pore size distributions of four samples are shown in Figure 2. Samples 64 and 72 have a wide range of pore sizes, with about half larger than 1 µm and half smaller than 1 µm, respectively. Samples 52 and 142 have a small range of pore size distributions, and the pores are mainly distributed below 1 µm.

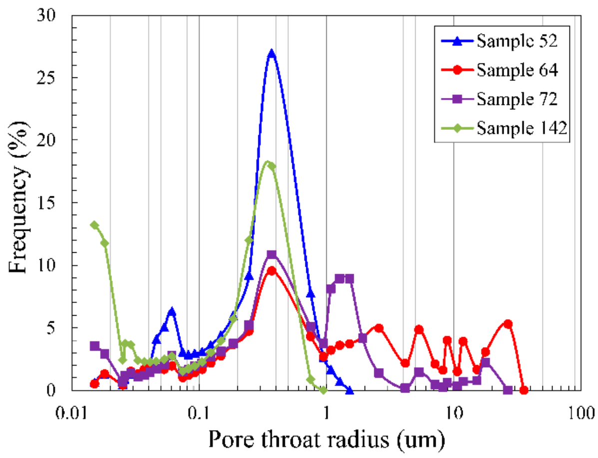

Figure 2. Pore size distributions of four samples obtained using mercury analysis.

4. Results and Discussion

4.1. Single Fractal Characteristics

Equation (1) was applied to obtain the fractal dimensions of the 13 mercury injection data. The results (Table 2) show that the high R-squared value demonstrates that fractal method is useful for mercury intrusion porosimetry (Figure 3). The fractal curves exhibit a two-stage characteristic and the corresponding fractal dimensions D_1 and D_2 can characterize the complexity of pore structure in different sizes. Despite the different pore size distributions, all 13 mercury intrusion curves exhibit a two-stage fractal characteristic. D_1 of 13 samples varies widely, while D_2 is mainly distributed around a value of 3.2.

Table 2. Parameters of the fractal dimension obtained from the 13 samples.

Samples	D_1	Correlation Coefficient R_2	D_2	Correlation Coefficient R_2	D_{sw}
9	5.1787	0.925	3.301	0.997	4.138
13	6.8716	0.946	3.302	0.985	4.592
22	5.9464	0.978	3.217	0.971	3.814
37	5.0279	0.920	3.319	0.957	4.092
46	7.1014	0.951	3.156	0.898	4.831
52	5.0715	0.948	3.276	0.939	3.989
64	4.1698	0.999	3.223	0.950	3.422
72	4.3472	0.927	3.195	0.968	3.638
81	4.8489	0.919	3.207	0.957	4.000
93	4.793	0.985	3.211	0.955	3.604
105	4.4449	0.998	3.216	0.989	3.636
142	6.3375	0.942	3.365	0.983	4.229
146	5.7515	0.992	3.281	0.999	4.367

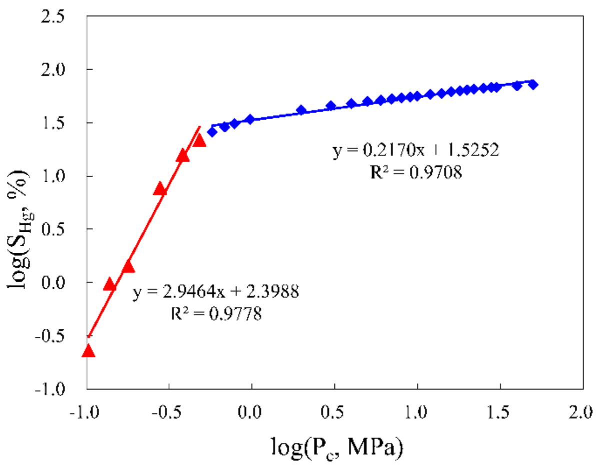

Figure 3. Plots of log(S_{Hg}) vs. log(P_c) from the mercury intrusion curve of sample 22.

To clarify the factors controlling the fractal dimension, pore size distributions of four samples are shown in Figure 4. Samples 64 and 72 have a wide range of pore size distributions, with about half of the pore volume larger than 1 μm and half less than 1 μm. Samples 52 and 142 have a small range of pore size distributions and the pores are mainly distributed below 1 μm. The mercury pressure of macropores is lower, meaning that a smaller fractal dimension can be obtained under the same mercury saturation condition. Therefore, the D_1 values of samples 64 and 72—4.1698 and 4.3472, respectively—are significantly larger than the D_1 value of samples 52 and 142, which are 5.0715 and 6.3375, respectively. Under the same conditions, the larger the proportion of large pores, the easier it is to obtain smaller fractal dimensions; this can be confirmed by examining the correlation between D_1 and r_{50}. D_1 has a good negative correlation with r_{50} when two abnormal points affected by microfractures are neglected. The ratio of larger pores volumes to total pore volumes acts as a control on the fractal dimension over a specific pore size range.

The sums of fractal dimensions D_1 of samples 13, 46, and 142 are 6.87, 7.10 and 6.34, respectively; these values are all beyond the theoretical value. Despite simultaneously considering the fractal dimension for pore space and tortuosity, the sum of fractal dimension D_1 may be greater than the theoretical value. Friesen's model, Angulo's model, Shen's model, and Su's model assume that only porous media are present in the reservoir and ignore the influence of microfractures. However, there may be microfractures in the samples, and the existence of the microfractures causes the abnormalities in the sum of fractal dimension D_1 [11].

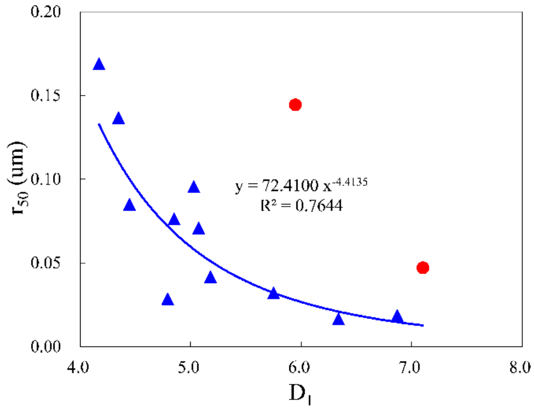

Figure 4. Plot of the sum of fractal dimension D_1 versus r_{50}.

4.2. Multifractal Characteristics

Multifractal analysis was conducted to describe the complexity of pore size distribution because single fractal theory has limitations in describing the local characteristics of pore size distribution. Figure 5 depicts the partition function for different q values in the double logarithmic coordinates of the four samples.

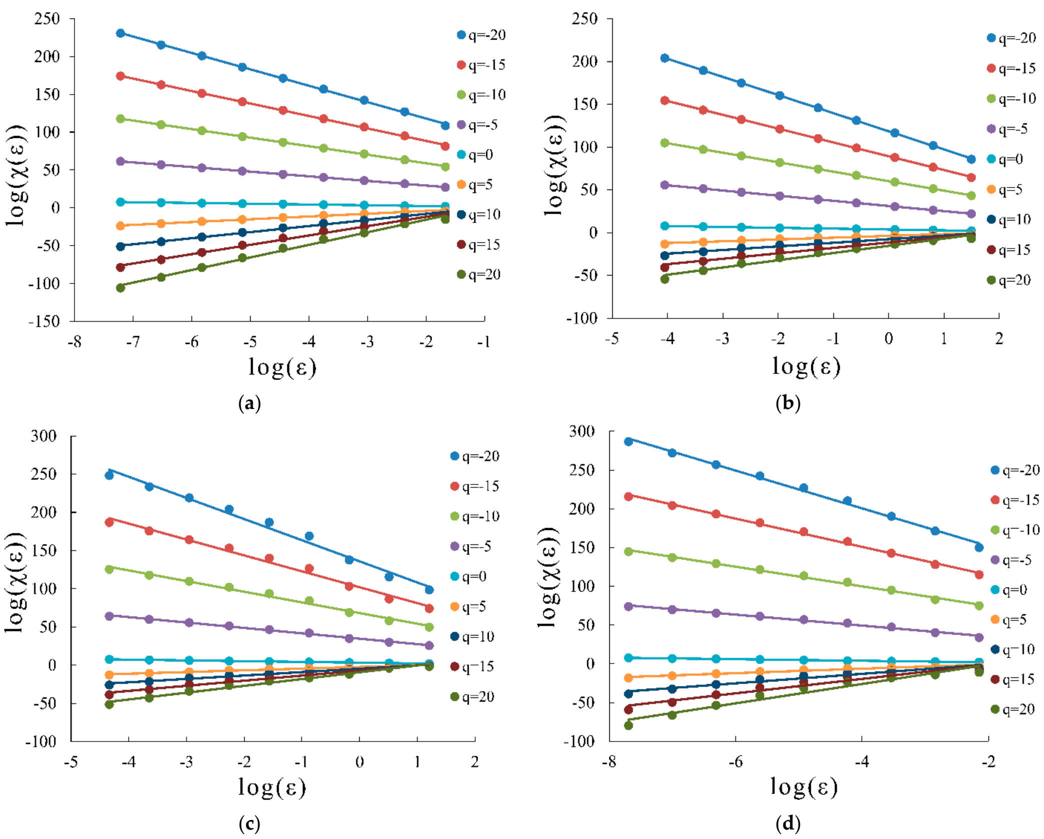

Figure 5. Plots of $\mu(\varepsilon)$ versus box size, ε, for the pore size distribution. (**a**) Sample 52; (**b**) Sample 64; (**c**) Sample 72; (**d**) Sample 142.

Linear relationships exist between log(ε) and log($\chi(\varepsilon)$) for the samples when $-20 \leq q \leq 20$ and the correlation coefficient is higher than 0.94 (Table 3). Favorable linear relationships between log(ε) and log($\chi(\varepsilon)$) indicate that the samples satisfy the multifractal characteristics. In accordance with Equation (4), the slopes of log(ε) and log($\chi(\varepsilon)$) are the mass exponent $\tau(q)$ The corresponding $\tau(q)$ increases when q increases from -20 to 20, indicating that the samples exhibit multifractal characteristics in a spatial distribution and that the multifractal method can be used to investigate the complexity and scale effects of pore size distribution.

Table 3. Coefficients for correlation determination R^2 of the fitting lines between log(ε) and log($\chi(\varepsilon)$).

q	Correlation Coefficient R^2			
	Sample 52	**Sample 64**	**Sample 72**	**Sample 142**
−20	0.9993	0.9999	0.9861	0.9947
−15	0.9994	0.9999	0.9870	0.9966
−10	0.9996	0.9999	0.9890	0.9978
−5	0.9998	1.0000	0.9945	0.9982
0	1.0000	1.0000	1.0000	1.0000
5	0.9957	0.9718	0.9829	0.9616
10	0.9937	0.9701	0.9820	0.9528
15	0.9928	0.9700	0.9820	0.9499
20	0.9924	0.9700	0.9820	0.9485

In accordance with Equation (6), the generalized dimension $D(q)$ was obtained in the range of $-20 \leq q \leq 20$. The relationship between the multifractal generalized dimension $D(q)$ and the moment order q is presented in Figure 6. The corresponding multifractal parameters are listed in Table 4. In the range of $-20 \leq q \leq 20$, the value of $D(q)$ when q is positive is less than the value of $D(q)$ when q is negative, thus indicating that regions with dense pore size distribution provides a better scale than the sparse regions. For a homogeneous fractal, the curves of $D(q)$ and q form a straight line, whereas those of non-uniform fractals have a certain width, and a large curvature indicates a poor homogeneity of samples. All four samples demonstrate a certain degree of curvature and exhibit a certain non-uniformity, but the curvatures were significantly greater in Samples 64 and 72 than in Samples 52 and 142, thereby demonstrating that Samples 64 and 72 are more heterogeneous in their pore size distribution.

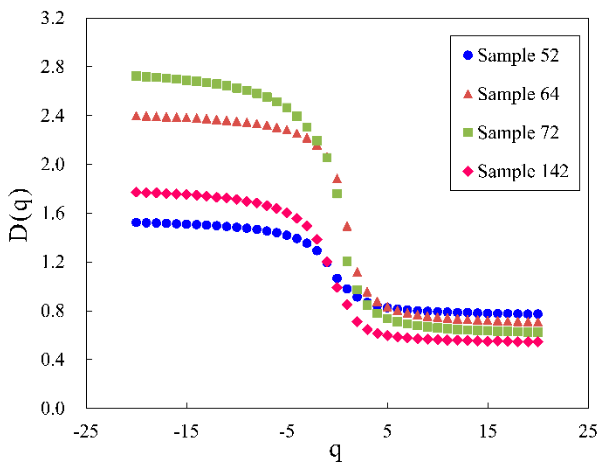

Figure 6. Plot of the multifractal generalized dimension $D(q)$ versus the moment order q.

Table 4. Multifractal dimension parameters obtained from the 13 samples.

Sample	$D(0)$	$D(1)$	$D(2)$	$D(1)/D(2)$	D_{min}	D_{max}	$\triangle D$
9	1.0082	0.9198	0.8314	0.9123	0.6934	1.3620	0.6686
13	0.9922	0.8695	0.7408	0.8764	0.5629	1.5441	0.9812
22	1.3816	1.1515	0.9762	0.8335	0.7323	2.1828	1.4506
37	1.0343	0.9346	0.8563	0.9036	0.7185	1.5000	0.7815
46	1.1469	1.0517	1.0171	0.9170	0.9096	1.6289	0.7193
52	1.0641	0.9773	0.9124	0.9185	0.7718	1.5227	0.7509
64	1.8827	1.4907	1.1157	0.7918	0.7073	2.3974	1.6901
72	1.7577	1.2061	0.9716	0.6862	0.6237	2.7235	2.0998
81	1.1421	0.9624	0.7910	0.8426	0.5907	1.6600	1.0692
93	1.3835	1.1169	0.8027	0.8073	0.5586	1.8413	1.2826
105	1.4816	1.1465	0.8809	0.7739	0.6233	2.1664	1.5431
142	0.9918	0.8520	0.7109	0.8590	0.5445	1.7734	1.2289
146	1.0658	0.9348	0.8195	0.8771	0.6215	1.4359	0.8144

Capacity dimension $D(0)$, information dimension $D(1)$, and correlation dimension $D(2)$ are listed in Table 4 [21]. A large capacity dimension $D(0)$ indicates a wide range of pore size distributions. The capacity dimensions of Samples 64 and 72 are 1.88 and 1.76, respectively, and are relatively larger than those for the 11 other samples. This indicates that the pore size distribution is large. A large pore size distribution suggests that large pores may be observed in the samples and may significantly improve the porosity and permeability of the reservoir; this condition can be confirmed by the large permeability and porosity of Samples 64 and 72.

The information dimension $D(1)$ reflects the degree of concentration of the pore size distribution, which represents the heterogeneity of pore structure. A large information dimension $D(1)$ indicates a highly heterogeneous pore size distribution. The information dimensions $D(1)$ of Samples 64 and 72 are relatively high, demonstrating that the unevenness of the pore size distribution is significant, and that pores are distributed over a wide range of pore sizes.

$D(1)/D(0)$ shows the dispersion of the pore size distribution. An added pore size is concentrated in the dense area when $D(1)/D(0)$ is close to 1, and the particle concentration in the sparse area is close to 0. The $D(1)/ D(0)$ values of Samples 64 and 72 are relatively minimal. This result shows that the pore size distribution of Samples 64 and 72 is discrete and is biased toward the sparse areas of the pore size distribution. The sparsely-grained area mainly refers to the area with large pore sizes in this study. This area can improve the physical properties and increase the seepage and storage capacities of the fluid in a reservoir despite the relatively minimal volume.

The multifractal spectrum of the 13 samples was calculated in accordance with Equations (10) and (11). Figure 7 illustrates the multifractal spectrum curves of the four samples. The multifractal spectrum functions a-$f(a)$ denote a continuous distribution, indicating that multifractal theory is a common phenomenon of the pore size distribution. Curves a-$f(a)$ are asymmetrical upward convex curves, which demonstrate that the local superposition of the different degrees during the formation of pores leads to the occurrence of reservoir heterogeneity.

In calculating the multifractal spectrum, the calculation domain is divided into different scales, with considerable scale information in the reservoir pore size distribution. Δa describes the characteristics of different regions, levels, and local conditions in a fractal structure. A large Δa value indicates a highly uneven distribution. The parameters of the multifractal spectrum are listed in Table 5. The value of Δa ranges from 0.7167 to 2.2413, with an average value of 1.2361. The maximum Δa of Sample 72 suggests that its heterogeneity is robust. By contrast, the smallest Δa of Sample 9 suggest that its heterogeneity is relatively weak.

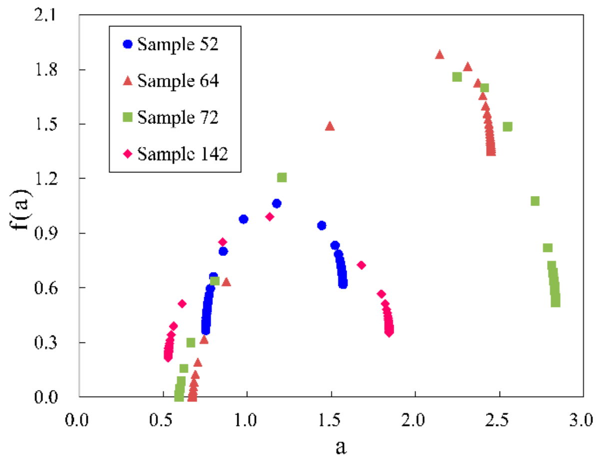

Figure 7. Plot of multifractal spectrum $f(a)$ versus the singularity strength a.

Table 5. Multifractal spectrum parameters obtained from the 13 samples.

Sample	a_{min}	a_{max}	$\triangle a$	$f(a_{min})$	$f(a_{max})$	$\triangle f(a)$	R	$f(a)_{max}$
9	0.6795	1.3962	0.7167	0.4158	0.6772	0.2614	0.1644	1.0082
13	0.5460	1.5946	1.0486	0.2234	0.5347	0.3113	0.1183	0.9922
22	0.7046	2.2587	1.5541	0.1782	0.6656	0.4874	0.2530	1.3816
37	0.7024	1.5436	0.8412	0.3967	0.6277	0.2311	0.0933	1.0343
46	0.8911	1.6651	0.7740	0.5395	0.9048	0.3653	0.0938	1.1469
52	0.7515	1.5680	0.8165	0.3654	0.6184	0.2530	0.0368	1.0641
64	0.6719	2.4498	1.7779	0.0003	1.3485	1.3482	0.6560	1.8827
72	0.5925	2.8338	2.2413	0.0000	0.5185	0.5185	0.4763	1.7577
81	0.5713	1.7032	1.1319	0.2018	0.7956	0.5938	0.3636	1.1421
93	0.5385	1.8867	1.3482	0.1557	0.9335	0.7778	0.5375	1.3835
105	0.5994	2.2303	1.6310	0.1442	0.8874	0.7432	0.4671	1.4816
142	0.5280	1.8444	1.3164	0.2142	0.3526	0.1384	-0.0823	0.9918
146	0.6001	1.4712	0.8711	0.1931	0.7297	0.5366	0.3952	1.0658

The equation Δf ($\Delta f = f(a_{min}) - f(a_{max})$) reflects the shape features of the multifractal spectrum. The shape of $f(a)$ depicts a right hook when the small probability subset dominates ($\Delta f < 0$). The shape of $f(a)$ illustrates a left hook when the large probability subset dominates ($\Delta f > 0$). The multifractal singularity curves in this study exhibit a right shape, indicating that the heterogeneity of the reservoir is mainly affected by the pore size distribution in the sparse region. This study emphasizes that large-scale pores contribute considerably to the spatial heterogeneity of a reservoir.

4.3. Relationship between Petrophysical and Single Fractal Parameters

The fractal dimensions D_1 and D_2 only characterize the complexity of pore structure in different sizes. The fractal dimension D_{sw} was introduced based on the weighted of the pore volume [28].

$$D_{sw} = D_1 \times S_{inf} + D_2 \times \left(S_{\max} - S_{inf}\right) \tag{12}$$

where S_{inf} is the inflection point saturation and $S_{\max}$ is the maximum saturation. D_{sw} can characterize the complexity of the whole pore size, and has a better correlation with petrophysical parameters (Figures 8 and 9). Larger D_{sw} values indicate that macropores and microfractures have greater influence on reservoir physical properties. The D_{sw} values is between 3.42 and 4.83, with average value of 4.03.

To explore the meaning of saturation-weighted fractal dimension D_{sw}, the correlations between D_{sw} and petrophysical parameters were investigated. D_{sw} has a good negative correlation with permeability (Figure 8), while D_{sw} has a good positive correlation with entry pressure (Figure 9). Permeability is an important indicator of reservoir quality; larger permeabilities are typically associated with high-quality reservoirs. The entry pressure is mainly influenced by the pore size; the smaller the pore size, the greater the entry pressure. Larger D_{sw} values indicate that the macropores are more heterogeneous, but this does not guarantee a larger volume of macropores or better reservoir properties. The correlations between D_{sw} and petrophysical parameters show that the increase of D_{sw} is accompanied by the decrease of pore size and permeability, resulting in poorer reservoir properties. Therefore, D_{sw} is a good indicator of reservoir quality.

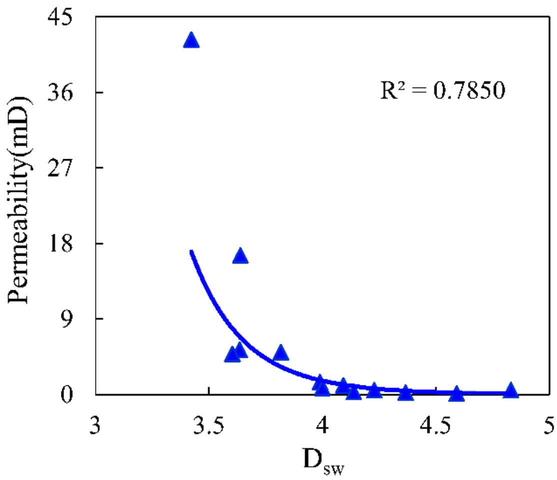

Figure 8. A plot of D_{sw} vs. permeability.

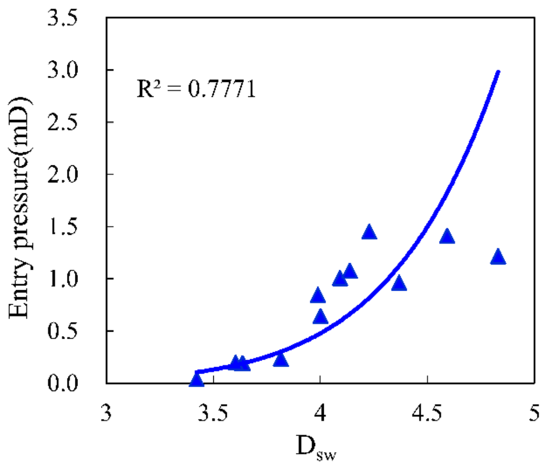

Figure 9. A plot of D_{sw} vs. entry pressure.

4.4. Relationship between Petrophysical and Multifractal Parameters

The relationships linking $D(0)$, $D(1)$, ΔD and Δf with permeability are determined to further explore the relationships between multifractal parameters and reservoir pore structure. Figure 10 shows that $D(0)$, $D(1)$, and ΔD are positively correlated with permeability, whereas Δf negatively correlates with permeability. $D(0)$ and $D(1)$ correlate well with permeability, with correlation coefficients of 0.8845 and 0.8665, respectively. $D(0)$ represents the range of the pore size distribution, and $D(1)$ characterizes the heterogeneity of the pore size distribution. The permeability improves with increasing $D(0)$ and $D(1)$. The more widely the reservoir particle size is distributed in the sparse region, the larger the reservoir size distribution range and the stronger the degree of heterogeneity. Therefore, the physical properties of the reservoir improve with increases in the range and heterogeneity of the pore size distribution.

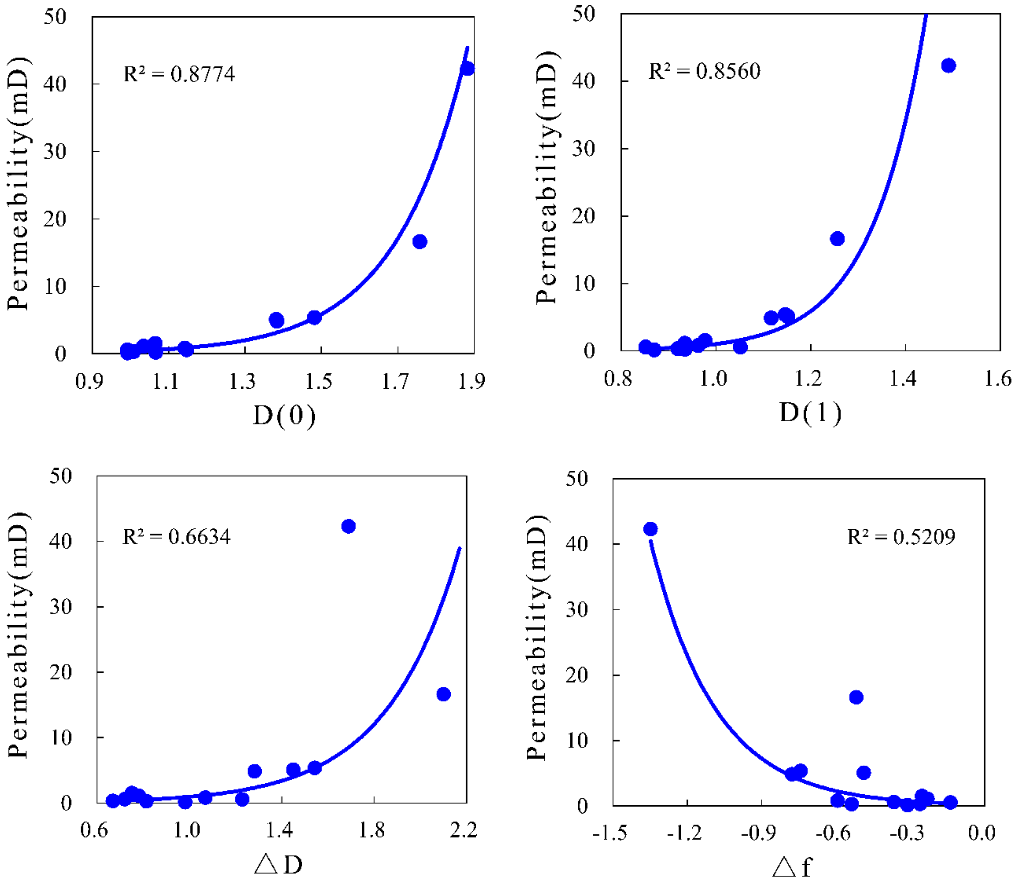

Figure 10. Plots of multifractal parameters and permeability.

Figure 11 presents the relationships linking $D(0)$, $D(1)$, ΔD, and Δf with the entry pressure. Favorable negative correlations exist between $D(0)$, $D(1)$, and ΔD and entry pressure, whereas Δf is positively correlated with entry pressure. Similarly, $D(0)$ and $D(1)$ correlate well with entry pressure, with correlation coefficients 0.9041 and 0.8971, respectively. $D(0)$ and $D(1)$ can be used as important parameters for characterizing and predicting physical properties of a reservoir.

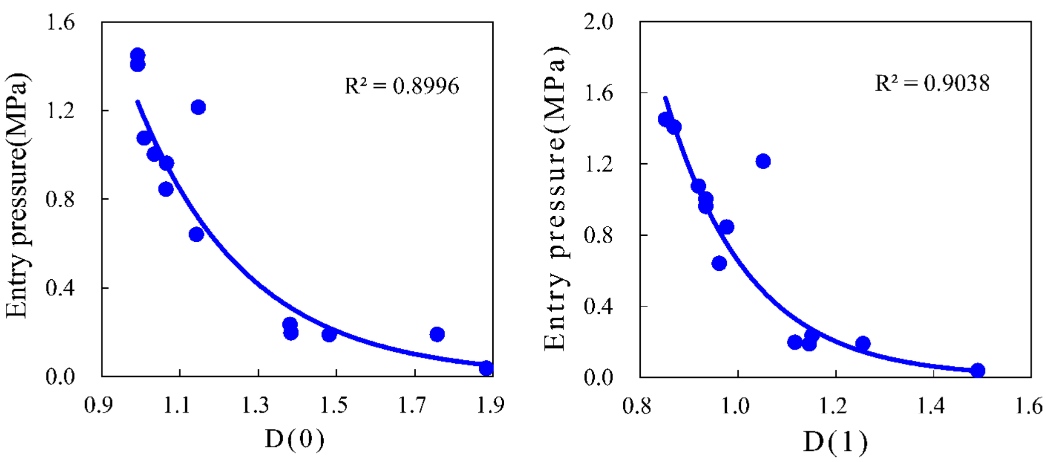

Figure 11. *Cont.*

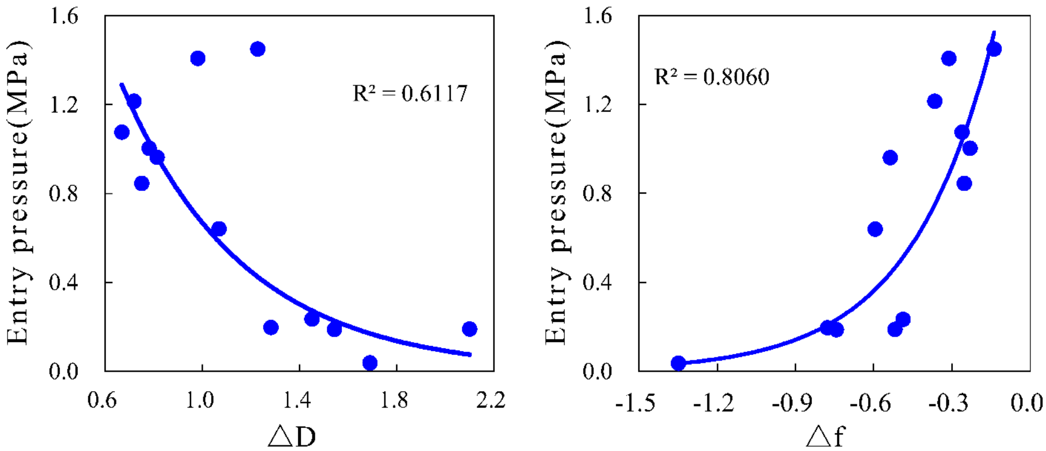

Figure 11. Plots of multifractal parameters and entry pressure.

4.5. Comparison between Single Fractal and Multifractal Analysis

Single fractal theory has been extensively used to characterize the heterogeneity of the pore structure, while multifractal analysis of mercury intrusion porosimetry in reservoir rocks is less commonly discussed. Comparative studies on single fractal and multifractal analysis are rare.

From the above analysis, we can see that there are some differences between single fractal and multifractal analysis. The D_{sw} values of samples 64 and 72 are lower than those of other samples, which generally implies that these two samples have low heterogeneity and good reservoir properties. However, samples 64 and 72 have bigger $D(0)$ and $D(1)$ values, as determined through multifractal analysis, demonstrating that these samples have a larger pore size distribution range and strong heterogeneity. Until now, this difference has not been observed or studied, since previous studies focus on the single or multifractal characteristics of mercury intrusion porosimetry. The difference is related to the fact that single fractal analysis and multifractal analysis characterize different aspects of the heterogeneity of a pore size distribution. The ratio of larger pores volumes to total pore volumes acts as a control on the fractal dimension over a specific pore size range, while the range of pore size distribution has the greatest effect on the multifractal analysis and multifractal parameters.

Single fractal theory characterizes the heterogeneity of pore structure from the entire range of pore sizes. The fractal curves show segmented fractal characteristics, and the fractal dimensions of each stage represents the complexity of the corresponding pore size range. The segmented fractal phenomenon demonstrates that multifractal theory is appropriate for describing fractal characteristics in a full-scale range. Multifractal theory is applied to explore pore size distribution in different scales. The pore structure exhibits multifractal characteristics in a local distribution, and the multifractal method can be used to investigate the complexity and scale effect of the pore size distribution.

It is worth noting that an intrinsic difference exists with respect to the single fractal models used to compute the fractal dimension. Friesen obtained a fractal model based on the Sierpinski carpet model [5]. The capillary bundle model was assumed in Shen's model [10]. Su set up a new fractal model considering of the fractal dimensions for pore space and tortuosity [11]. Different fractal dimensions may be obtained when these different fractal models are applied [29]. Moreover, the fractal dimension of the low pressure stage may exceed the theoretical value. This is because the current fractal models assume that the reservoir is composed only of pores and ignore the influence of microfractures. It has been confirmed that the presence of microfractures can significantly increase the fractal dimension [30]. Multifractal analysis explores pore size distribution characteristics without any a priori assumptions, considering the effect of microfractures.

We show that fractal analysis and multifractal analysis are feasible means for characterizing the heterogeneity of pore structures in a reservoir. By comparing the relationships between single fractal and multifractal parameters and reservoir physical parameters, we learn that multifractal parameters have better correlations with reservoir physical properties than single fractal parameters. The aforementioned factors combined mean that multifractal analysis is more suitable for characterizing the heterogeneity of a pore size distribution when the pore size distribution of the samples is addressed without any a priori assumptions.

5. Conclusions

In this study, single fractal and multifractal theory were applied to investigate pore size distribution characteristics of reservoir rocks as well as the influences of the single fractal and multifractal parameters on pore structure. The following conclusions can be drawn from our work:

(1) The single fractal curves exhibit segmented fractal characteristics and the fractal dimensions of the low-pressure section is greater than the fractal dimension of the high-pressure section. The saturation-weighted fractal dimension D_{sw} has a better correlation with permeability and entry pressure than D_1 or D_2.
(2) Linear relationships exist between $\log(\varepsilon)$ and $\log(\mu,(\varepsilon))$ for the 13 samples when $-20 \leq q \leq 20$, suggesting that the pore structures of the 13 samples exhibit multifractal characteristics. Multifractal parameters $D(0)$ and $D(1)$ correlate well with permeability and entry pressure. The physical properties of the reservoir improve with increases in the range of pore size distribution.
(3) The ratio of larger pores volumes to total pore volumes acts as a control on the fractal dimension over a specific pore size range, while the range of pore size distribution has the greatest effect on the multifractal analysis and multifractal parameters.
(4) Fractal analysis and multifractal analysis are feasible methods for characterizing the complexity of pore size distribution in a reservoir. Multifractal analysis with parameters $D(0)$ or $D(1)$ produce better correlations with reservoir physical properties. In conclusion, multifractal analysis is more suitable for characterizing the heterogeneity of pore size distributions when the pore size distribution of samples is addressed without any a priori assumptions.

Author Contributions: P.S. analyzed the experiment data and wrote the paper; Z.X. provide core samples and designed the study; P.W. polished English; W.D. deduced formulas; Y.H. drawn figures; W.Z. searched literatures; Y.P. organize article format.

Funding: The research has been founded by the National Science and Technology Major Project of China (2016ZX05029005).

Conflicts of Interest: The authors declare no conflict of interest.

References

1. Li, W.; Liu, H.; Song, X. Multifractal analysis of Hg pore size distributions of tectonically deformed coals. *Int. J. Coal Geol.* **2015**, *144*, 138–152. [CrossRef]
2. Ghanbarian, B.; Hunt, A.G.; Daigle, H. Fluid flow in porous media with rough pore-solid interface. *Water Resour. Res.* **2016**, *52*, 2045–2058. [CrossRef]
3. Pfeifer, P.; Avnir, D. Chemistry in noninteger dimensions between two and three. I. Fractal theory of heterogeneous surfaces. *J. Chem. Phys.* **1983**, *79*, 3558–3565. [CrossRef]
4. Katz, A.J.; Thompson, A.H. Fractal sandstone pores: Implications for conductivity and pore formation. *Phys. Rev. Lett.* **1985**, *54*, 1325–1328. [CrossRef] [PubMed]
5. Friesen, W.I.; Mikula, R.J. Fractal dimensions of coal particles. *J. Colloid Interface Sci.* **1987**, *120*, 263–271.
6. Hu, J.; Tang, S.; Zhang, S. Investigation of pore structure and fractal characteristics of the Lower Silurian Longmaxi shales in western Hunan and Hubei Provinces in China. *J. Nat. Gas Sci. Eng.* **2016**, *28*, 522–535. [CrossRef]
7. Chen, X.; Yao, G.; Cai, J.; Huang, Y.; Yuan, X. Fractal and multifractal analysis of different hydraulic flow units based on micro-CT images. *J. Nat. Gas Sci. Eng.* **2017**, *48*, 145–156. [CrossRef]
8. Lei, G.; Cao, N.; Liu, D.; Wang, H. A Non-Linear Flow Model for Porous Media Based on Conformable Derivative Approach. *Energies* **2018**, *11*, 2986. [CrossRef]

9. Angulo, R.F.; Alvarado, V.; Gonzalez, H. Fractal dimensions from mercury intrusion capillary tests. In Proceedings of the SPE Latin America Petroleum Engineering Conference, Caracas, Venezuela, 8–11 March 1992.
10. Shen, P.; Li, K. A new method for determining the fractal dimension of pore structures and its application. In Proceedings of the 10th Offshore South East Asia Conference, Singapore, 6–9 December 1994.
11. Su, P.; Xia, Z.; Qu, L.; Yu, W.; Wang, P.; Li, D.; Kong, X. Fractal characteristics of low-permeability gas sandstones based on a new model for mercury intrusion porosimetry. *J. Nat. Gas Sci. Eng.* **2018**, *60*, 246–255. [CrossRef]
12. Stanley, H.E.; Meakin, P. Multifractal phenomena in physics and chemistry. *Nature* **1988**, *335*, 405. [CrossRef]
13. Lai, J.; Wang, G.; Fan, Z.; Chen, J.; Wang, S.; Zhou, Z.; Fan, X. Insight into the pore structure of tight sandstones using NMR and HPMI measurements. *Energy Fuels* **2016**, *30*, 10200–10214. [CrossRef]
14. Jiang, F.; Chen, D.; Chen, J.; Li, Q.; Liu, Y.; Shao, X.; Dai, J. Fractal analysis of shale pore structure of continental gas shale reservoir in the ordos basin, NW China. *Energy Fuels* **2016**, *30*, 4676–4689. [CrossRef]
15. Peng, C.; Zou, C.; Yang, Y.; Zhang, G.; Wang, W. Fractal analysis of high rank coal from southeast Qinshui basin by using gas adsorption and mercury porosimetry. *J. Pet. Sci. Eng.* **2017**, *156*, 235–249. [CrossRef]
16. Martínez, F.S.J.; Martín, M.A.; Caniego, F.J.; Tuller, M.; Guber, A.; Pachepsky, Y.; García-Gutiérrez, C. Multifractal analysis of discretized X-ray CT images for the characterization of soil macropore structures. *Geoderma* **2010**, *156*, 32–42. [CrossRef]
17. Jouini, M.S.; Vega, S.; Mokhtar, E.A. Multiscale characterization of pore spaces using multifractals analysis of scanning electronic microscopy images of carbonates. *Nonlinear Process. Geophys.* **2011**, *18*, 941–953. [CrossRef]
18. Subhakar, D.; Chandrasekhar, E. Reservoir characterization using multifractal detrended fluctuation analysis of geophysical well-log data. *Phys. A Stat. Mech. Its Appl.* **2016**, *445*, 57–65. [CrossRef]
19. Ferreiro, J.P.; Vázquez, E.V. Multifractal analysis of Hg pore size distributions in soils with contrasting structural stability. *Geoderma* **2010**, *160*, 64–73. [CrossRef]
20. Xie, S.; Cheng, Q.; Ling, Q.; Li, B.; Bao, Z.; Fan, P. Fractal and multifractal analysis of carbonate pore-scale digital images of petroleum reservoirs. *Mar. Pet. Geol.* **2010**, *27*, 476–485. [CrossRef]
21. Wang, P.; Jiang, Z.; Ji, W.; Zhang, C.; Yuan, Y.; Chen, L.; Yin, L. Heterogeneity of intergranular, intraparticle and organic pores in Longmaxi shale in Sichuan Basin, South China: Evidence from SEM digital images and fractal and multifractal geometries. *Mar. Pet. Geol.* **2016**, *72*, 122–138. [CrossRef]
22. Zhao, P.; Wang, Z.; Sun, Z.; Cai, J.; Wang, L. Investigation on the pore structure and multifractal characteristics of tight oil reservoirs using NMR measurements: Permian Lucaogou Formation in Jimusaer Sag, Junggar Basin. *Mar. Pet. Geol.* **2017**, *86*, 1067–1081. [CrossRef]
23. Liu, K.; Ostadhassan, M. Quantification of the microstructures of Bakken shale reservoirs using multi-fractal and lacunarity analysis. *J. Nat. Gas Sci. Eng.* **2017**, *39*, 62–71. [CrossRef]
24. Zheng, Q.; Yu, B. A fractal permeability model for gas flow through dual-porosity media. *J. Appl. Phys.* **2012**, *111*, 024316. [CrossRef]
25. Yu, B.; Li, J. Some fractal characters of porous media. *Fractals* **2001**, *9*, 365–372. [CrossRef]
26. Ge, X.; Fan, Y.; Li, J.; Zahid, M.A. Pore structure characterization and classification using multifractal theory—An application in Santanghu basin of western China. *J. Pet. Sci. Eng.* **2015**, *127*, 297–304. [CrossRef]
27. Wang, J.; Zhang, M.; Bai, Z.; Guo, L. Multi-fractal characteristics of the particle distribution of reconstructed soils and the relationship between soil properties and multi-fractal parameters in an opencast coal-mine dump in a loess area. *Environ. Earth Sci.* **2015**, *73*, 4749–4762. [CrossRef]
28. Liu, K.; Ostadhassan, M.; Kong, L. Fractal and multifractal characteristics of pore throats in the Bakken Shale. *Transp. Porous Media* **2019**, *126*, 579–598. [CrossRef]
29. Zhang, T.; Li, X.; Li, J.; Feng, D.; Wu, K.; Shi, J.; Han, S. A fractal model for gas–water relative permeability in inorganic shale with nanoscale pores. *Transp. Porous Media* **2018**, *122*, 305–331.
30. Lai, J.; Wang, G. Fractal analysis of tight gas sandstones using high-pressure mercury intrusion techniques. *J. Nat. Gas Sci. Eng.* **2015**, *24*, 185–196. [CrossRef]